Magnetic skyrmions and bimerons in films with anisotropic interfacial Dzyaloshinskii-Moriya interaction

O. G. Udalov, I. S. Beloborodov, and M. V. Sapozhnikov

Phys. Rev. B **103**, 174416 — Published 13 May 2021

DOI: 10.1103/PhysRevB.103.174416

Magnetic skyrmions and bimerons in films with anisotropic iDMI

O. G. Udalov,[1,2,3] I. S. Beloborodov,[2] and M. V. Sapozhnikov[1,3]

[1] *Institute for Physics of Microstructures RAS, Nizhny Novgorod, 603950, Russia*
[2] *Department of Physics and Astronomy, California State University Northridge, Northridge, CA 91330, USA*
[3] *Lobachevsky State University of Nizhny Novgorod, 603950 Nizhny Novgorod, Russia*

(Dated: April 27, 2021)

We consider localized topologically non-trivial magnetic textures - skyrmions, antiskyrmions and bimerons in a thin magnetic film with anisotropic interfacial Dzyaloshinskii-Moriya interaction (iDMI). We use micromagnetic simulations and analytical consideration for studying of the internal magnetic structure and stability of these textures. Skyrmion and antiskyrmion become elliptic and orient along the main axes of the iDMI tensor even for small anisotropy. In contrast, bimeron (antibimeron) orientation changes fluently with varying the iDMI anisotropy. Depending on the iDMI anisotropy the bimeron may consist of vortex and antivortex pair or of "hedgehog" state and antivortex. In experiment the considered iDMI anisotropy can be induced by a strain applied to a magnetic film. We develop a phenomenological approach to establish the strain-iDMI relation.

PACS numbers: 75.50.Tt 75.75.Lf 75.30.Et 75.75.-c

I. INTRODUCTION

Recently, topologically non-trivial magnetization distributions rise a lot of attention due to their unique physical properties and promising applications [1–12]. These spin textures may appear either in a crystal with broken inversion symmetry or in an artificial multilayer structure consisting usually of ferromagnet (FM) and heavy metal (HM) films [13]. At now, several types of topological magnetic solitons are known. The most studied is the skyrmion (Sk) appearing in HM/FM multilayers with perpendicular magnetic anisotropy [13–18]. In the absence of external magnetic field the skyrmion is stabilized by the interfacial Dzyaloshinskii-Moriya interaction (iDMI). The counter-partner of the skyrmion is the antiskyrmion (aSk). While Sk can appear in systems with isotropic iDMI, the aSk requires the anisotropic iDMI. They were predicted [19 and 20] and observed [21 and 22] in several crystals (and epitaxial films) with certain symmetry. In artificial structures HM/FM, aSk can appear only if the iDMI has opposite sign along different directions [23 and 24]. So far, fabrication of such films were not reported and aSk was not observed in artificial systems. A topological analogue of magnetic Sk in-easy plain films is magnetic bimeron. Their possible existence in the films with iDMI was recently theoretically predicted [25–32].

Using magnetic solitons in applications requires an effective way of creating, annihilating and moving these textures in thin films. This is still challenging task nowadays and many groups are working on the issue currently. The approach based on spin-polarized currents [29, 30, 33–40] requires huge current density about 10^7 A/cm^2 making it not relevant for applications. This motivate people to develop strain and charge mediated approaches [41–46].

Recently, it was experimentally shown that the iDMI can be controlled in a wide range with a strain in artificial magnetic multilayer films [47 and 48]. Since the iDMI is responsible for stabilization of topological texture, the strain can be used to manipulate them. Interestingly, the strain induces not only the iDMI strength variation but also the iDMI anisotropy. Moreover, under certain strain the iDMI can have a different sign along different directions. An isotropic film where Sk may exist can be transformed to the film with strong anisotropic iDMI favouring aSk formation. Therefore it is interesting to study the behavior of Sk and aSk as a function of iDMI anisotropy. Note that the anisotropic strain can be induced with electric field in the hybrid system FM-ferroelectric as shown in Fig. 1. A FM film hosts topological magnetic structure and serves as an electrode. Applying a voltage to the FE substrate one can create a deformation using piezoelectric effect. These deformations are transferred into FM film and induce the DMI anisotropy.

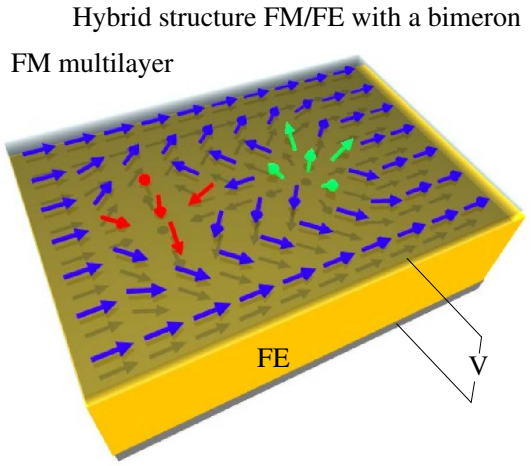

FIG. 1. Sketch of a ferromagnetic/ferroelectric hybrid structure. A bimeron is situated in the FM film. A voltage V is applied across the ferroelectric layer inducing a strain in the ferromagnetic film affecting the iDMI.

A skyrmion is stabilized by the iDMI in artificial multilayers. In films with isotropic iDMI a Sk represents a cylindrically symmetric magnetization distribution. The size of the skyrmion depends on the iDMI strength [49]. For small iDMI ($D < D_{\rm col}$) the skyrmion collapses. The critical value of iDMI ($D_{\rm col}$) is usually found numerically. When the iDMI exceeds the energy of the domain wall (DW), $D > D_{\rm cr} \approx W_{\rm DW}/\pi = 4\sqrt{AK}/\pi$, a separate skyrmion experiences runout instability (here A is the exchange stiffness and K is the film anisotropy constant). For intermediate region, $D_{\rm col} < D < D_{\rm cr}$, a separate skyrmion can exist.

Skyrmions in the magnetic film with anisotropic iDMI were discussed in Ref. [50] where stability of a single Sk depending on the applied magnetic field and iDMI anisotropy was studied for zero magnetic anisotropy. In the absence of magnetic anisotropy a Sk is unstable without an external magnetic field. It was shown that iDMI anisotropy leads to less stable skyrmions. In addition, the long-range magneto-dipole (MD) interaction was not taken into account.

A magnetic aSk in an artificial film is less studied theoretically. In Ref. [24] the case of magnetic film with iDMI of opposite sign along x- and y-directions ($D_x = -D_y$, where $D_{x,y}$ are the iDMI coefficients along two orthogonal directions in the film plane) was discussed. It was shown that the aSk is cylindrically symmetric for zero (or weak) dipole-dipole interaction in this case. The stability criterion for an aSk as a function of iDMI anisotropy was not studied.

Bimerons (Bi) may appear due to competing exchanges without the iDMI interaction as shown in Ref. [27]. Occurrence of a Bi lattice in thin film with in-plane anisotropy and iDMI was shown in Ref. [26]. Stabilization of a single Bi due to iDMI in a thin film with in-plane magnetic anisotropy was discussed in Refs. [30 and 31]. A stability diagram for a Bi in the isotropic FM layer was obtained using micromagnetic simulation. Similarly to Sk and aSk, the Bi exists in a narrow range of iDMI values. When the domain wall energy becomes negative a single bimeron disappears transforming to stripe domains or a magnetic helix. This defines the upper bound for the iDMI strength. At small enough iDMI the Bi collapses. Due to isotropy of the film the bimeron consists of a pair of "hedgehog" state (with positive winding number) and antivortex (with negative winding number).

In this work we investigate stability and magnetic structure of localized topologically non-trivial states in the thin magnetic films as a function of iDMI anisotropy. We consider skyrmion, antiskyrmion and bimeron using micromagnetic simulations and semi-analytical approaches. In our model we take into account all interactions relevant to realistic experimental systems such as perpendicular anisotropy and long-range MD interaction.

The paper is organized as follows. First, we present the results of micromagnetic simulations of the stability of Sk, aSk and Bi in a magnetic film with anisotropic iDMI in Sec. II. Then, we discuss the main peculiarities of the stability diagrams using analytical models in Sec. III. Finally, we discuss a possibility to create the anisotropic iDMI with electric field and provide a phenomenological consideration of iDMI-stain relation in Sec. IV.

II. MICROMAGNETIC SIMULATIONS OF TOPOLOGICALLY NON-TRIVIAL MAGNETIC TEXTURES IN FILMS

A. The model and micromagnetic simulations procedure

We consider a thin uniform ferromagnetic film with saturation magnetization $M_{\rm s}$, thickness t, and exchange stiffness A. The film has a perpendicular (interfacial or magneto-crystalline) magnetic anisotropy with volume energy density $W_{\rm an} = -K(\mathbf{m}\mathbf{z}_0)^2$, where $\mathbf{m}$ is the unit vector along the film magnetization, $\mathbf{z}_0$ is the film normal and K is the magnetic anisotropy constant, $K > 0$. Note that the effective magnetic anisotropy including the shape contribution, $K_{\rm eff} = K - \mu_0 M_{\rm s}^2/2$ (μ_0 is the vacuum permeability, $K_{\rm eff}$ units are energy/length^3) can be either positive or negative. If $K_{\rm eff} > 0$ the energy of the state with uniform out-of-plane magnetization ("OOP" state) is less than the energy of the state with uniform in-plane magnetization ("IP" state). There is also iDMI in the film. Its energy is

$$W_{\rm DMI} = \\ = D_x\left(m_x\frac{\partial m_z}{\partial x} - m_z\frac{\partial m_x}{\partial x}\right) + D_y\left(m_y\frac{\partial m_z}{\partial y} - m_z\frac{\partial m_y}{\partial y}\right). \quad (1)$$

Here D_x, D_y are iDMI coefficients along x- and y-axes. There is no magnetic anisotropy axis in the film plane. However, the film can be anisotropic due to anisotropic iDMI ($D_x \neq D_y$). We study localized nonuniform states shown in Fig. 2. Here we denote them as skyrmion (Sk), antiskyrmion (aSk), bimeron (Bi) and antibimeron (aBi). The Sk and Bi states have the same topology and carry the same topological charge [51]

$$N_{\rm ch} = \frac{1}{4\pi}\int \mathbf{m}\cdot\frac{\partial \mathbf{m}}{\partial x}\times\frac{\partial \mathbf{m}}{\partial y} = 1, \quad (2)$$

The Bi can be obtained from Sk by rotating the magnetization by 90 degrees around the y-axis, see Fig. 2. Such rotation does not change the topological charge of the system. Antibimeron and aSk have the topological charge equal to -1. The aBi can be obtained from aSk by rotating magnetization by 90 degrees.

Below we use the following definitions for (a)Sk and (a)Bi. By Sk (Fig. 2) we mean a *localized* magnetic state with a topological charge +1 and vorticity +1 in a film magnetized in negative z direction. The *localized* state with a topological charge of -1 and vorticity of -1 is considered as aSk. The *localized* topologically charged states

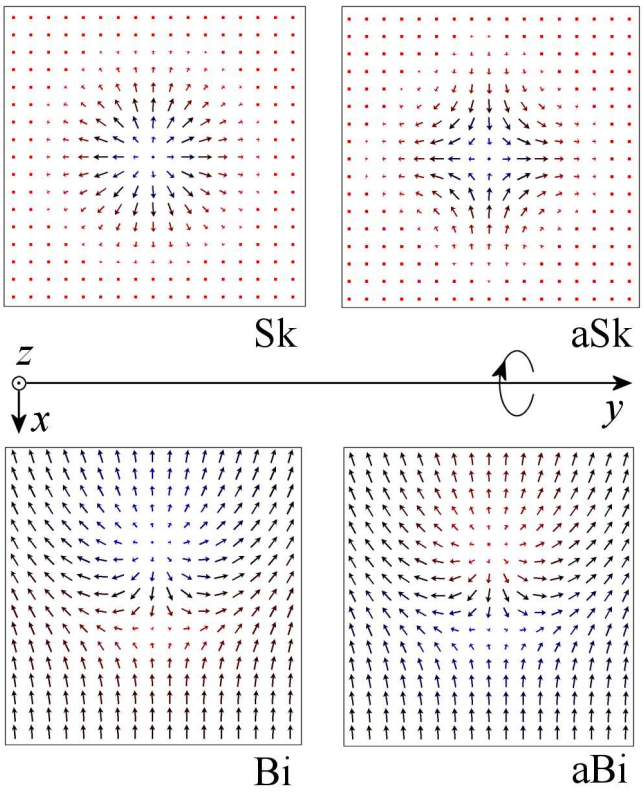

FIG. 2. Localized topological states: Sk and aSk stand for skyrmion and antiskyrmion, respectively; Bi and aBi stand for bimeron and antibimeron. The blue and red colors denote positive and negative values of M_z, respectively.

with +1 and -1 charges in the easy-plane films are considered as Bi and aBi, respectively. The Bi consists of closely spaced center and saddle points (Fig. 2, Bi). In the aBi the magnetization direction m_z is opposite at these points (Fig. 2, aBi).

Micromagnetic simulations are performed utilizing the OOMMF code [52] to solve the problem of Sk and Bi stability. This code is based on a numerical solution of the system of Landau-Lifshitz-Gilbert (LLG) equations for the magnetization of the system.

$$\frac{\partial \vec{M}}{\partial t} = -\gamma(\vec{M} \times \vec{H}_{eff}) - \frac{\gamma\alpha_0}{M_s}[\vec{M} \times (\vec{M} \times \vec{H}_{eff})], \quad (3)$$

where M is the magnetization, γ is the gyromagnetic ratio, α_0 is the dimensionless damping parameter, and M_s is the saturation magnetization. The effective field $\vec{H}_{eff} = -\delta E/\delta \vec{M}$ is a variation derivative of the energy function. The total energy of the system is defined by

$$E = E_{ex} + E_K + E_m + E_{DM}. \quad (4)$$

The first term E_{ex} is the energy of the exchange interaction. The second term E_K is the energy of the uniaxial anisotropy, E_m is the demagnetization energy. Expressions for these terms and corresponding effective fields

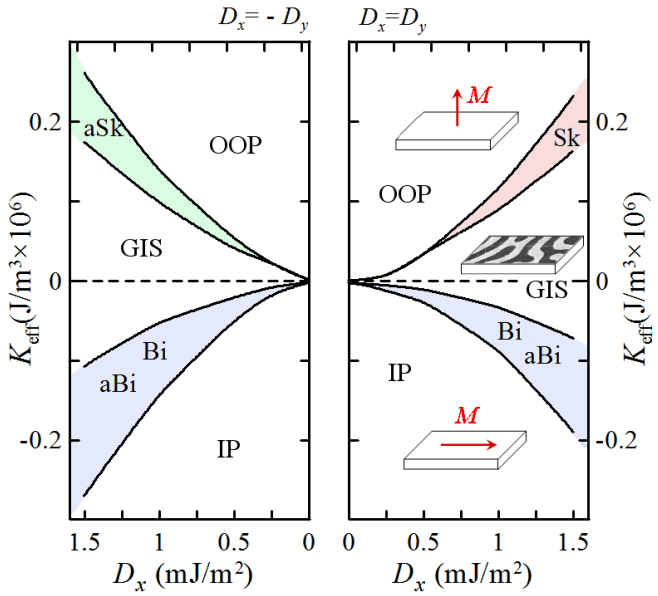

FIG. 3. Stability diagram of localized topological states. Right panel is for isotropic iDMI. Left panel is for anisotropic iDMI with $D_x = -D_y$. OOP stands for out-of-plane magnetization. IP stands for in-plane magnetization. GIS stands for globally inhomogeneous state.

have conventional form and can be found in Refs. [53–55]

The simulated system is the rectangular plate with the width of 762 nm and the thickness of $t = 1$ nm which is typical value for the Co/Pt bilayers. Periodical boundary conditions in the plane of the film are used. The mesh element size $1.5 \times 1.5 \times 1$ nm^3 is much smaller than the DW width.

In our calculations we use typical material parameters for ferromagnetic films with a perpendicular anisotropy. The stiffness constant is chosen as $A = 1.6 \cdot 10^{-11}$ J/m and $M_s = 1300$ kA/m. We initialize our film introducing one of the topologically non-trivial configuration as a nucleons and let the system evolve to equilibrium. Depending on the system parameters the initial state may disappear (collapse) leading to a uniform magnetized state. Another scenario is when the initial localized magnetic state experienced runout instability and the system turns into some globally inhomogeneous state (GIS). In both these cases we consider the topological texture as unstable. If at the end of the magnetization evolution the localized magnetic texture survives we consider it as stable.

B. Phase diagram in coordinates (K,D) for isotropic film

The stability diagram of magnetic film with isotropic iDMI ($D_x = D_y$) is shown in the right panel in Fig. 3. There are several regions in the diagram. A Sk exists

only in a small sector in the upper right quadrant. This quadrant corresponds to the out-of-plane effective magnetic anisotropy. For fixed magnetic anisotropy there is a narrow range of iDMI values where a Sk is stable. This is in agreement with previous studies. The Sk collapses (Sk→OOP transition) with increasing anisotropy K or decreasing D_x. The collapse is accompanied by a change in the topological charge. Therefore, this phase boundary can be accurately defined. The collapse is not reversible. Changing K or D_x cannot transform the uniform state to a topologically charged one.

A Sk experiences runout instability and turns into GIS with decreasing K or increasing of D_x. This is due to decrease of the DW energy in this case. Sk → GIS transition conserves the value of topological charge. Therefore, this transformation is reversible. The opposite change of K or D values transforms the GIS to a localized Sk. We define this boundary when a significant Sk expansion occurs.

The upper quadrant of the left panel in Fig. 3 shows the stability region for an aSk at $D_x = -D_y$. The region resembles the one for a Sk. Note that there is no intersection of Sk and aSk stability regions and they cannot coexist in the same film.

Bi and aBi exist only in the bottom part of the diagram for $K_{\text{eff}} < 0$. In contrast to Sk and aSk, the Bi and aBi may co-exist in the same film and in both limits $D_x = D_y$ and $D_x = -D_y$. When Bi (aBi) collapses, it irreversibly transforms to the state with uniform in-plane (IP) magnetization. The transformation to GIS is reversible.

Note that there is an essential difference between the pair Sk-aSk and Bi-aBi. The Bi and aBi can be transformed one into another using the system rotation by the angle π around the x-axis. Therefore, the energy of Bi and aBi is the same. This is not the case for Sk and aSk: the system rotation cannot transform Sk to aSk.

C. Stability diagram of skyrmions and antiskyrmions in films with anisotropic iDMI

To study the influence of the iDMI anisotropy we fix the K constant and vary iDMI constants D_x and D_y independently. The stability diagram of skyrmions and antiskyrmions in coordinates (D_x,D_y) is shown in Fig. 4 for $K = 1.16 \cdot 10^6$ J/m^3 ($K_{\text{eff}} = 1.03 \cdot 10^5$ J/m^3). All other material parameters were defined before. The stability diagram is symmetric with respect to the line $D_x = D_y$. This is because the replacement $D_{x,y} \to D_{y,x}$ is equivalent to rotation of the system by 90 degrees which does not affect the skyrmions stability conditions. Similarly, the diagram is symmetric with respect to the line $D_x = -D_y$.

A single Sk can be stable only in the region $D_x D_y > 0$ within a narrow "triangle" around the point $D_x = D_y = 1$ mJ/m^2. The case of isotropic film (considered in previous works) corresponds to the diagonal $D_x = D_y$. As we discussed in the introduction there is an upper and

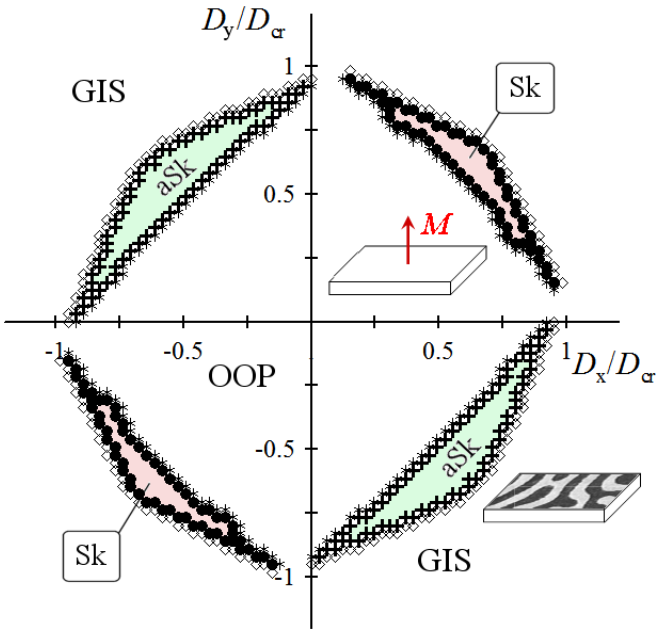

FIG. 4. Stability diagram for a single Sk and aSk in film with anisotropic iDMI. Single Sk is stable for $D_x D_y > 0$. An aSk exists in the second and fourth quadrants ($D_x D_y < 0$) only. Closed circles and crosses show the boundary points where Sk or aSk are stable. Open diamonds and stars show the first points outside of the stability region. OOP stands for out-of-plane magnetization. GIS stands for globally inhomogeneous state. $D_{\text{cr}} = 4\sqrt{AK_{\text{eff}}}/\pi \approx 1.6\text{mJ/m}^2$.

lower bounds for iDMI magnitude in this case. If iDMI is higher than the upper bound a Sk expands and transforms into some GIS. Such a GIS can be a labyrinth domain structure or lattice of magnetic bubbles. Below the lower bound a Sk collapses and the film becomes uniformly magnetized.

We introduce the average iDMI strength as $D = \sqrt{D_x^2 + D_y^2}$ and the anisotropy as $\xi_{\text{an}} = |D_x|/|D_y|$. Using this definition the case $D_x = -D_y$ is isotropic. When iDMI is anisotropic ($\xi_{\text{an}} \neq 1$) the range of average iDMI values D in which skyrmions can exist shrinks. For high enough iDMI anisotropy ($\xi_{\text{an}} > 10$ or $\xi_{\text{an}} < 0.1$) there is no iDMI values giving Sk stabilization. However, in the film with anisotropic iDMI the upper bound for iDMI along one of the directions is higher than for isotropic case. So, a single Sk can survive at higher iDMI value. One can see, that the line for Sk-OOP boundary is practically straight and have a slope of -1. As for the Sk-GIS boundary, it's slope is $-1/2$ and $-3/2$. So, the upper bound for D_x at $D_y \approx 0$ is about 1.5 times higher than critical D_x along the line $D_x = D_y$.

A single aSk can exist only in the second and forth quadrants ($D_x D_y < 0$) when iDMI has different sign along different directions. So, a Sk and an aSk cannot coexist in a thin film according to our simulations. The region of parameters where an aSk survives also resem-

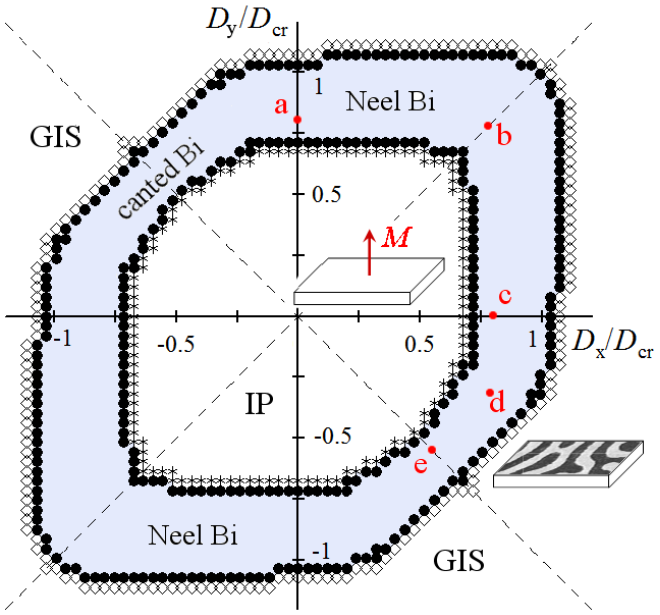

FIG. 5. Stability diagram for bimerons (Bi) in film with anisotropic iDMI. Points show coordinates at which the magnetization distributions are simulated in Fig. 6. Closed circles and stars show the Bi to uniform state transition (collapse). Open diamonds and closed circles show transition of Bi to the globally inhomogeneous state (GIS). IP stands for in-plane magnetization. $D_{cr} = 4\sqrt{A|K_{eff}|}/\pi \approx 1.25$ mJ/m^2.

bles a triangle. The upper bound for iDMI strength is lower for aSk than for Sk. This is related to the difference of their internal structure. The DW in the Sk is of Neel type. In the aSk the DW changes it's type from Bloch to Neel type as one moves around the aSk. This makes the MD energy of the DW different for Sk and aSk. The latter is smaller leading to faster transformation of the aSk into GIS as we increase the iDMI strength. The stability of the aSk and Sk is discussed on the base of simplified model in Sec. III.

D. Stability diagram of Bi and aBi in films with anisotropic iDMI

Similarly to Sk and aSk, we study the stability of single Bi and aBi in the film with anisotropic iDMI. We simulate a magnetic film with in-plane effective magnetic anisotropy $K = 1.001\cdot10^6$ J/m^3 ($K_{eff} = -6.1\cdot10^4$ J/m^3). Other parameters are the same as in the previous section. Figure 5 shows such a diagram in coordinates (D_x,D_y). A single Bi is stable between the lines resembling ellipses. Similar to Sk and aSk there is upper and lower critical values of iDMI strength D for Bi stability. In contrast to Sk, a single Bi can be stable in all quadrants $D_xD_y > 0$ and $D_xD_y < 0$. The stability region in the first (third) quadrant is different from the one in the fourth (second) quadrant. The average iDMI D is lower in region $D_xD_y < 0$. This is due to different internal structure of the DW in Bi in these two cases. The DWs for $D_xD_y < 0$ have lower energy since both iDMI and MD energies are minimized. We discuss this in more details in Sec. III G. The magnetization distribution in Bi for different iDMI anisotropy is shown in Fig. 6. In all cases the Bi represents a pair of "saddle" point and "center" point. The saddle point (which is an antivortex) keeps its structure for any ratios of D_x an D_y values. Contrary, the helicity (angle θ between the magnetization and a radius vector from the center point) of the center point depends on this ratio. For $D_xD_y > 0$ there is a "hedgehog" structure with $\theta = 0$ (Fig. 6(a-c)) while for $D_x = -D_y$ there is vortex with $\theta = \pm\pi/2$ (Fig. 6(e)). For intermediate values of D_x an D_y there is a canted structure ($0 < |\theta| < \pi/2$, Fig. 6(d)). The ratio of D_x and D_y determines also the orientation of the Bi. The orientation is characterised by the vector $\mathbf{q}$ which connects the saddle and center points. It is oriented by the angle ϕ_q with respect to the x-axis. Another important angle characterizing the Bi (ϕ_M) is the orientation of magnetization far from the Bi. Angles ϕ_q and ϕ_M seems to be related as $\phi_q = -\phi_M$. For $D_x = D_y$ the system is isotropic and Bi can have any orientation. For $D_x > 0$ and $D_y > 0$ the Bi is oriented along the direction of strongest iDMI. For D_x and D_y of different signs the vector $\mathbf{q}$ begin to tilt reaching the value $\phi_q = \pm\pi/4$ at $D_x = -D_y$. In this case, the Bloch DWs appear in the Bi lowering both MD and iDMI energies. Importantly, there is no crystallographic anisotropy in the film plane in the considered system. Therefore, the uniform magnetization surrounding a Bi can be oriented in either direction and does not force the Bi to be directed in a certain way. Due to the rotational degeneracy of the uniform state, the orientation of the Bi is defined by it's DW structure. So, the uniform magnetization surrounding a Bi adjusts to the Bi orientation. In real samples there is always some in-plane anisotropy and DW pining sites preventing this behaviour. It is interesting to note that the correlation between Bi orientation and its internal structure in the film with anisotropic iDMI resembles the correlation between orientation and internal structure of the equilibrium DW in similar system [56].

The difference between aBi and Bi is due to magnetization direction in the cores of the nodes only. Therefore, the Bi and aBi have the same energy (for the same system parameters). Thus, the stability diagram for a single aBi is the same as for a single Bi and we do not show it here. The Bi and aBi can coexist in the same film in contrast to Sk and aSk.

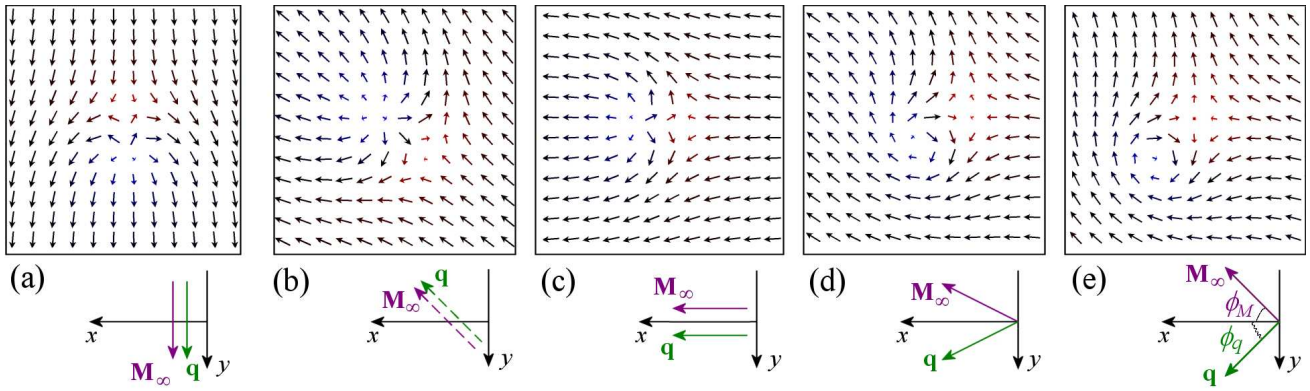

FIG. 6. The structure and orientation of a bimeron state for different ratios of D_x and D_y. The specific values of iDMI constants corresponding to Figs. (a)-(e) are denoted by red dots in Fig. 5. Bottom row shows the orientation of magnetization far from the Bi ($\mathbf{M}_\infty$) and the vector connecting "center" and "saddle" points of the Bi ($\mathbf{q}$).

III. ANALYTICAL CONSIDERATION OF TOPOLOGICAL STATES IN FILMS WITH ANISOTROPIC IDMI

A. The model

Here we consider the influence of iDMI anisotropy on shape, internal structure and stability of topologically non-trivial magnetic textures in a bilayer structure FM/HM. The properties of these textures are defined by the competition of the several energy contributions: 1) exchange interaction; 2) magnetic anisotropy; 3) MD interaction; and 4) iDMI. We consider a thin (thinner than the exchange correlation length) magnetic film with the thickness t and saturation magnetization M_s. The film plane is perpendicular to the z-axis. The magnetization is uniform along the z-direction. The system has a uniaxial magnetic anisotropy along the z-axis, which may occur due to the interfacial effects (as in Co/Pt films). The anisotropy energy is the same as in Sec. II A. The exchange energy density is given by $W_\mathrm{ex} = A((\partial\mathbf{m}/\partial x)^2+(\partial\mathbf{m}/\partial y)^2+(\partial\mathbf{m}/\partial z)^2)$. The iDMI is defined by Eq. (1). Besides the demagnetizing factor the MD interaction leads to two additional contributions to the soliton energy: i) due to charges in the DW of the soliton and ii) due to the interaction of the core of the topological structure (bounded by the DW) with the surrounding magnetic film (the region outside the DW).

B. Skyrmion model

A single Sk in isotropic film has a circularly symmetric magnetization distribution. For the anisotropic iDMI we consider a Sk as an ellipse with two radii, a and b and the orientation angle α (see Fig. 7). Following Ref. [49], we consider a Sk with the size larger than the characteristic DW width $a, b \gg \Delta = \sqrt{A/K_\mathrm{eff}}$. In this case, the Sk can be represented as a DW of an elliptical shape. The DW with the width Δ is bounded by the dashed lines in Fig. 7. with the center shown by the blue solid line. Inside the ellipse the magnetization is uniform and directed perpendicular to the film plane. Outside of the ellipse the magnetization looks the opposite direction.

Consider a small part of the Sk DW shown in Fig. 7(c). The DW is oriented along the local ellipse normal, $\mathbf{n}$. Note that this normal is not co-directed with the radius vector $\mathbf{r}$ connecting Sk center and the considered local point. We introduce the angle γ between $\mathbf{n}$ and $\mathbf{r}$ (see Fig. 7(b)). The angle between the main ellipse axis and the considered local point is φ. Finally, one can see that the domain wall is oriented by the angle $\gamma+\varphi+\alpha$ with respect to the x axis. One can find the angle γ as follows

$$\gamma = \mathrm{arccot}(b^2/a^2\mathrm{ctg}(\varphi)) - \varphi. \tag{5}$$

The length of the considered segment is given by

$$dl = \frac{rd\varphi}{\cos(\gamma)}, \tag{6}$$

where the radius of the ellipse in the considered point is defined by

$$r = \frac{ab}{\sqrt{b^2\cos^2(\varphi)+a^2\sin^2(\varphi)}}. \tag{7}$$

The internal structure of the DW for anisotropic iDMI was considered in Ref. [56], where it was shown that anisotropic iDMI leads to the formation of mixed type of DW (intermediate between Bloch and Neel types). The energy of the DW per unit length is given by

$$W_\mathrm{DW} = t\left(\frac{2A}{\Delta} + 2K_\mathrm{eff} - \pi D_+\cos(\theta) - \right.$$
$$\left. -\pi D_-\cos(2(\alpha+\varphi+\gamma)-\theta) + \frac{1}{2}k\Omega\cos^2(\theta)\right), \tag{8}$$

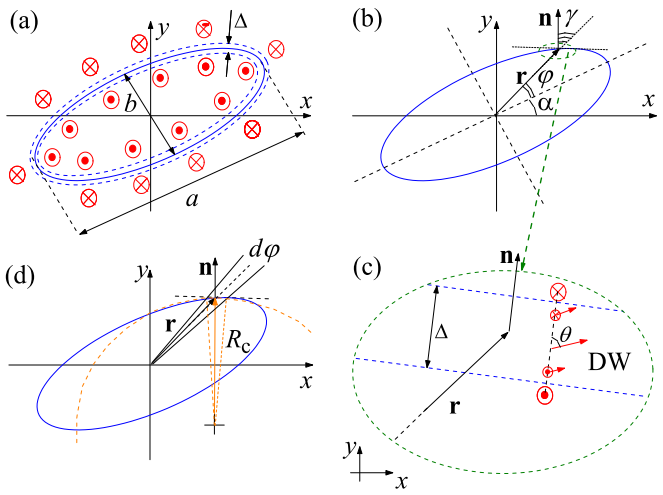

FIG. 7. Sketch of a Sk. The solid blue line corresponds to zero out-of-plane magnetization. The dashed blue lines show the DW size Δ. a and b are the ellipse dimensions. The red arrows show magnetization in the Sk. The vector $\mathbf{n}$ is the normal to the Sk surface (blue line). r is the distance between the Sk center and the DW. α is the Sk orientation angle. γ is the angle between the Sk normal $\mathbf{n}$ and radius vector $\mathbf{r}$. R_c is the Sk local curvature radius. (c) shows the internal structure of the DW of the Sk. θ is the orientation of magnetization rotation plane.

where the first two terms describe the exchange energy and the magnetic anisotropy energy. The third and fourth terms are the iDMI contribution with

$$D_+ = \frac{D_x + D_y}{2},\ D_- = \frac{D_x - D_y}{2}. \tag{9}$$

The angle θ defines the orientation of magnetization rotation plane (see Fig. 7(c)). For $\theta = 0,\pi$ one has the Neel DW, while for $\theta = \pm\pi/2$ the DW becomes of the Bloch type. The last term in Eq. (8) describes the contribution from the MD energy of magnetic charges in the DW with $\Omega = \mu_0 M_s^2 t$ and $k \approx 0.44$.

For isotropic film we have $D_+ = D_x = D_y$ and $D_- = 0$ and the DW becomes of the Neel type with $\theta = 0$ (when the iDMI is stronger than the MD interaction). The iDMI anisotropy makes the DW of mixed Bloch-Neel type.

For given Sk shape the DW orientation $(\gamma + \varphi + \alpha)$ is fixed, therefore we need to minimize the energy in Eq. (8) with respect to θ only.

$$\frac{\partial W_{\rm DW}}{\partial \theta} = 0, \tag{10}$$

giving $\theta_{\rm min}(\varphi)$ the orientation of the magnetization rotation plane in a local DW as a function of the position of the DW in the Sk. For negligible MD contribution the angle is given by

$$\theta_{\rm min} = \operatorname{atan}\left(\frac{2D_- \sin(2(\gamma+\alpha+\varphi))}{D_+ + 2D_- \cos(2(\gamma+\alpha+\varphi))}\right). \tag{11}$$

For non-zero MD interaction ($\Omega > 0$) the analytical solution for $\theta_{\rm min}$ is not possible and the angle should be found numerically.

The total energy of the DW in the whole Sk is found by the integration over the angle φ

$$W_{\rm DW}^{\rm tot} = t\int_0^{2\pi} d\varphi \frac{abW_{\rm DW}(\theta_{\rm min})}{\cos(\gamma)\sqrt{b^2\cos^2(\varphi) + a^2\sin^2(\varphi)}}. \tag{12}$$

Since the DW in the Sk is bended an additional term appears in the energy due to the DW curvature. It is produced by the exchange interaction and is due to magnetization derivatives with respect to the angle φ. Using approach of Ref. [49] for a cylindrically symmetric Sk, we can write for the elliptic Sk

$$W_{\rm c}^{\rm tot} = 2tA\Delta\int_0^{2\pi} d\varphi \frac{(\partial\gamma/\partial\varphi + 1)r}{R_c^2\cos(\gamma)}, \tag{13}$$

where R_c is the curvature radius (see Fig. 7(d)) given by

$$R_{\rm c} = \frac{(a^2\sin^2(\omega) + b^2\cos^2(\omega))^3}{ab}, \tag{14}$$

with ω being

$$\omega = \arctan\left(\frac{a}{b}\tan(\varphi)\right). \tag{15}$$

The last contribution to Sk energy is due to the long-range part of the MD interaction. The Sk can be represented as a domain with opposite magnetization. The domain presence reduces the MS interaction comparing to a uniformly magnetized film. For a cylindrically symmetric "bubble" domain with the radius r the energy gain is given by [57]

$$W_{\rm MD}^{\rm round} = -\pi\Omega t^2 I(d), \tag{16}$$

where $d = 2r/t$ and

$$I(d) = \frac{2}{3\pi}d\left(d^2 + (1-d^2)\frac{E(v^2)}{v} - \frac{K(v^2)}{v}\right). \tag{17}$$

The functions E and K are the complete elliptical integrals and $v^2 = d^2/(1+d^2)$. For elliptic Sk the energy in Eq. (16) is transformed to the one obtained in Ref. [57]

$$W_{\rm MD}^{\rm tot} = \frac{1}{2\pi}\int_0^{2\pi} W_{\rm MD}^{\rm round}(d(\varphi)). \tag{18}$$

The total Sk energy is

$$W_{\rm Sk}(a,b,\alpha) = W_{\rm c}^{\rm tot} + W_{\rm DW}^{\rm tot} + W_{\rm MD}^{\rm tot}. \tag{19}$$

Minimizing the energy over parameters a, b and α one can find the Sk size and orientation.

C. Critical iDMI for cylindrical skyrmion

For circularly symmetric Sk ($a = b$) one can analytically estimate the upper bound for iDMI at which a single Sk experiences a runout instability. The DW energy is given by $W_{\rm DW}^{\rm tot} = 2\pi a(4\sqrt{AK_{\rm eff}} - \pi D + k\Omega/2)$ (we assume that $D_x > k\Omega/\pi$). The energy of the DW curvature is given by $W_{\rm c}^{\rm tot} = 4\pi A\Delta/a$. While the long-range MD contribution can not be presented with a simple function, the derivative of the MD energy with respect to the Sk radius a can be calculated using an approximate expression $\partial W_{\rm MD}^{\rm tot}/\partial a \approx -8\pi\Omega t(a/t)^N\alpha/3$ valid for $a \gg t$, Ref. [58]. In this reference, for the parameter region they consider $N = 0$ and $\alpha = 1$. In our parameters region the better approximation is given by $N = 2/15$ and $\alpha = 0.92$. Finally, we obtain an equation for equilibrium Sk radius

$$a_{\rm Sk} = \sqrt{\frac{2A\Delta}{4\sqrt{AK_{\rm eff}} - \pi D + k\Omega/2 - 4\Omega\varkappa/3}}, \qquad (20)$$

where

$$\varkappa = \alpha\left(\frac{3A\Delta}{\alpha\Omega N}\right)^{N/(2+N)}. \qquad (21)$$

The Sk radius diverges when the iDMI coefficients tend to the critical value

$$D_{\rm cr}^{\rm Sk} = 4(\sqrt{AK_{\rm eff}} + k\Omega/8 - \Omega\varkappa/3)/\pi, \qquad (22)$$

Divergence of Sk radius means that the Sk is unstable and transforms into a GIS. One can see that the short-range part of MD energy of the Sk domain wall increases the Sk stability range while the long-range MD interaction decreases it. The contribution of the long-range MD interaction is larger than that of the short-range one. Eventually, the MD interaction reduces the upper bound of the Sk stability, since the MD interaction favours a multidomain state in a film with perpendicular anisotropy.

D. Critical iDMI coefficients for anisotropic film

For the anisotropic iDMI the simulations show that the Sk shape is circularly symmetric and the ratio $a/b \approx 1$. Therefore, we find the criterion for Sk stability with circular shape in a film with anisotropic iDMI. Equations (13) and (12) are simpler for this case. The energy of the DW curvature transforms to $W_{\rm c}^{\rm tot} = 4\pi aA\Delta$. The long-range MD interaction is defined by Eq. (16). Eventually, we arrive to the following criterion for the Sk stability

$$-\delta W_{\rm DW} < 4(\sqrt{AK_{\rm eff}} - \Omega\varkappa/3), \qquad (23)$$

where the energy $\delta W_{\rm DW}$ is the iDMI and local MD energy averaged over the Sk domain wall

$$\delta W_{\rm DW} = \frac{-1}{2}\int_0^{2\pi} d\varphi(D_+\cos(\theta) + D_-\cos(2\varphi-\theta) - \frac{k\Omega}{2\pi}\cos^2(\theta)). \qquad (24)$$

Here θ depends on φ and is defined by minimization of expression in the integral.

For typical parameters of magnetic multilayers the critical value of iDMI coefficient are larger than Ω and we can neglect the last term in Eq. (24). In this case

$$\tan(\theta) = \frac{D_-\sin(2\varphi)}{D_+ + D_-\cos(2\varphi)}. \qquad (25)$$

For isotropic iDMI we obtain Eq. (22). We can also calculate the critical D_x for strongly anisotropic case of $D_x \neq 0$ and $D_y = 0$. In this case $\theta = \varphi$ and we get the following critical iDMI

$$D_{\rm cr}^{\rm an} = 4(\sqrt{AK_{\rm eff}} - \Omega\varkappa/3 + k\Omega/8)/2. \qquad (26)$$

One can see that D_x for strongly anisotropic iDMI is approximately 1.5 time larger than the critical D_x for isotropic case. This is in agreement with our simulations in Fig. 4.

E. Analytical phase diagram of a single skyrmion in films with anisotropic iDMI

For arbitrary shape Sk we minimize Eq. (19) over angle α and sizes a and b numerically to find if skyrmion is stable or not. The Sk is unstable if energy $W_{\rm Sk}$ does not have a minimum as a function of a and b. The stability diagram obtained by minimizing Eq. (19) is shown in Fig. 8. It is calculated for $A = 1.6 \cdot 10^{-11}$ J/m, $M_{\rm s} = 1300$ kA/m, $K = 1.2 \cdot 10^6$ J/m^3 and film thickness $t = 1$ nm. The parameters are similar to the ones used in micromagnetic simulations.

First, we minimize over the angle α and find that $\alpha = 0$ meaning that the Sk main axes are co-directed with the main axes of the strain. At that, the short axis is oriented along the direction with higher iDMI. So, only two parameters, a and b depend on D_x and D_y. Therefore, the stability diagram shows the dependence of equilibrium Sk ellipticity a/b and the Sk energy, $W_{\rm Sk}$ as a function of D_x and D_y. The blue area shows the region where Sk is unstable. The line between the blue and the multicolor region corresponds to the upper bound for the iDMI constants. The lower bound can not be obtained using the continuum model considered above and occurs only in a discrete model.

Note that replacement $D_{x,y} \to D_{y,x}$ leads to the transformation $a \to b$, $b \to a$ and $W_{\rm Sk} \to W_{\rm Sk}$. Therefore, we plot the ratio a/b only in the upper half of the figure and use the lower part to show the dependence of Sk energy on iDMI constants.

One can see that the ellipticity is small, ($a/b \approx 1$), in almost all area of the Sk stability. It only increases in a very close vicinity to the stability line meaning that the iDMI can be strongly anisotropic while the skyrmion is still cylindrically symmetric. Therefore, our assumption about the Sk shape in Sec. III C is valid. Dashed green

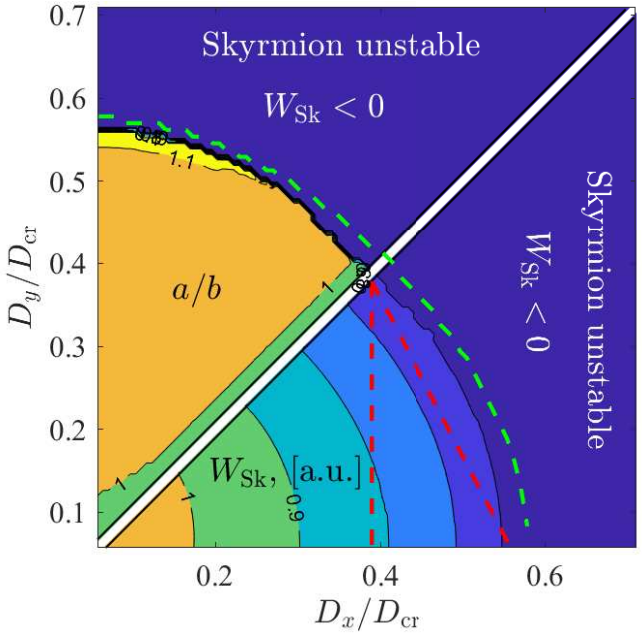

FIG. 8. Ellipticity (upper part) and energy of a single Sk (in arbitrary units, bottom part) as a function of iDMI constants along x- and y-directions. Since the substitution $D_{x,y} \to D_{y,x}$ does not affect the Sk energy we plot the ellipticity in upper part and energy in the bottom part. In the blue region a Sk is not stable. The line splitting blue region and multicolor region is the upper bound for the iDMI strength. As discussed in the text the bottom boundary for $D_{x,y}$ cannot be defined from the analytical model. So, the data for small $D_{x,y}$ are irrelevant for real systems. $D_{\rm cr} = 4\sqrt{AK_{\rm eff}}/\pi$. The green dashed line shows the upper bound for iDMI strength given by Eq. (23).

line shows the threshold for iDMI constants obtained using Eq. (23) for cylindrical Sk. One can see that the model of circular Sk leads to slightly larger threshold for iDMI coefficient.

Comparing Fig. 4 and Fig. 8 one sees that the stability boundaries obtained with analytical model and micromagnetic simulations are in a qualitative agreement. Note that the value of anisotropy constant K is close to the transition between in-plane and out-of-plane magnetization orientation. In this region the critical iDMI is very sensitive to the system parameters. So, small changes in K or $M_{\rm s}$ lead to a wide range of values of parameter $D_{\rm cr}$. This could be a reason for discrepancy between the analytical stability diagram and the one obtained using micromagnetic simulations.

As it was discussed in Sec. II C, the upper bound curve in (D_x, D_y) coordinates resembles a straight line with the slope -3/2 (or -1/2). We plot a (dashed red) line with the slope -3/2 starting from the upper bound point for isotropic case. At $D_y = 0$ this line gets exactly to the upper bound of Sk stability. So, we can conclude that analytical model leads to a qualitatively similar stability diagram.

Note that while the shape of a Sk is almost circularly symmetric the orientation of magnetization rotation plane in a Sk domain wall is not circularly symmetric. This is due to the anisotropic iDMI and partially due to the magneto-static interaction. For isotropic case the DW is the same in all directions. For large enough $D_{x,y}$, it is of Neel type. For strong anisotropy ($D_x \neq 0$ and $D_y \approx 0$) the DW along the x direction is of the Neel type and is of the Bloch type along the y direction. So, while the shape of a Sk is not affected by the iDMI anisotropy the internal structure is modified.

The Sk energy is also shown as a function of D_x and D_y. The energy decays with increasing the iDMI strength. This is because the Sk energy depends on the DW energy which decreases with increasing the iDMI. One can see that it decays as a function of average iDMI strength, D.

While the analytical approach cannot describe the collapse of a Sk, we can still give an explanation of the Sk-OOP boundary shape. As we mentioned the ratio $a/b \approx 1$ meaning that Sk is practically cylindrically symmetric. In this case the iDMI and MD energy are reduced to Eq. (24). In this equation however the orientation of magnetization rotation plane is defined by the competition of the MD and iDMI energies. This is valid for large Sk with large curvature radius (the case of Skyrmion→GIS transition). The collapse happens in the opposite limit when the curvature radius is very small. In this limit the exchange interaction dominates. It defines the DW internal structure. Due to the exchange interaction the angle θ becomes fixed in the whole domain wall lowering the exchange interaction. In this case Eq. (24) simplifies even more leading to $\delta W_{\rm DW} = -\pi D_+ \cos(\theta)/2 + k\Omega \cos^2(\theta)/2$. This means that the Sk-OOP boundary in (D_x,D_y)-plane is defined by D_+ and happens at some line $D_x + D_y = const$. This is what we have in numerical simulations in Fig. 4.

F. Anti-skyrmion with anisotropic iDMI interaction

An aSk exists in the system with iDMI of different sign along x- and y-directions. As shown in Ref. [24] for $D_x = -D_y$ the aSk has a circularly symmetric shape. One can expect that the shape is slightly distorted for $D_x \neq -D_y$ (similarly to the case of Sk). Therefore, to study the case of arbitrary iDMI coefficient we consider an elliptical aSk. The aSk energy ($W_{\rm aSk}$) has the same contributions as the Sk one. The aSk DW energy is given by Eq. (12). The angle θ is found using energy minimization. Due to different sign of DMI along different directions the orientation of magnetization rotation plane θ behaves differently comparing to a Sk. Angle θ makes a turn counter-clockwise when φ makes a clockwise rotation. The DW curvature energy is given by Eq. (13). The long-range MD energy is also similar to Sk case and is given by Eq. (16). This term describes the energy of

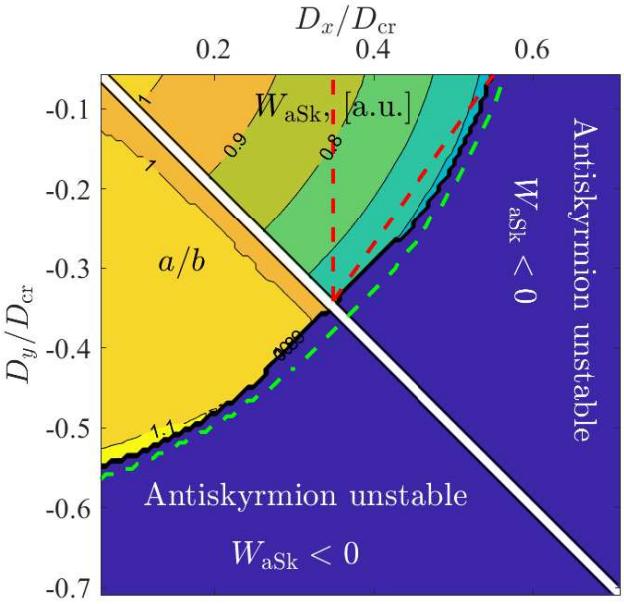

FIG. 9. Ellipticity (lower part) and energy (in arbitrary units, upper part) of a single aSk as a function of iDMI along the x- and y-directions. Since the $D_{x,y} \to D_{y,x}$ change does not affect aSk energy we plot the ellipticity in lower part and the energy in the upper part. In the blue region the aSk is unstable. The line splitting blue region and multicolor region is the upper bound for the aSk stability. As discussed in the text the bottom boundary for $D_{x,y}$ cannot be defined from the analytical model. So, the data for small $D_{x,y}$ are not relevant for real systems. $D_{cr} = 4\sqrt{AK_{eff}}/\pi$. The green dashed line shows the upper bound of iDMI strength given by Eq. (23).

interaction of the internal part of an aSk with the magnetic film surrounding the aSk. However, in contrast to Sk there is an additional contribution to the aSk long-range MD energy. Due to opposite rotation direction of the angle θ, magnetic charges in the aSk DW form a quadrupole magnetic moment. In the present consideration we neglect this term. Performing the same minimization procedure for parameters region $D_x > 0$ and $D_y < 0$ we find the stability of an aSk.

Figure 9 shows the stability diagram for an aSk similar to Fig. 8 for Sk. All parameters are the same as in the previous section for Sk. One can see that the upper threshold is lower comparing to Sk case. This is in agreement with the micromagnetic simulations (Fig. 4). To understand this we first consider the case of $D_x = -D_y$. We also assume that $\pi D_x \gg k\Omega/2$ which is correct for iDMI value close to the aSs-GIS transition. In this case $\theta \approx 2\varphi$. Introducing this solution into the DW energy of an aSk we find $W_{DW}^{aSk} = 4\sqrt{AK_{eff}} - \pi D_x - k\Omega/4$. Comparing this expression to the energy of the Sk DW (Sec. III C), one can see that the aSk DW energy is lower than that of Sk by $k\Omega/4$. This is because the magnetic charges produced by the aSk varies with angle φ and give lower MD energy. In Sk the charge is the same along the whole DW. The contribution to the aSk energy due to the DW curvature and long-range MD interaction is the same as for Sk. Therefore, the critical iDMI value for aSk is lower. For $D_x = -D_y$ it is given by

$$D_{cr}^{aSk} = 4(\sqrt{AK_{eff}} + k\Omega/16 - \Omega\varkappa/3)/\pi. \qquad (27)$$

One can see that the ellipticity of aSk is very small. So, we can use the circular symmetry to estimate the upper boundary for iDMI coefficients and Eqs. (23) and (24) can be used to calculate the critical iDMI for aSk. The green dashed line in Fig. 9 shows the critical iDMI obtained using Eqs. (23) and (24) for aSk.

G. Bimerons in films with anisotropic iDMI

While analytical consideration of Bi is more difficult than for Sk and aSk, the main features of the Bi stability diagram (obtained in micromagnetic simulations) can be understood using simplified arguments.

The first peculiarity of the stability diagram (Fig. 5) is that Bi can exist for both cases $D_xD_y > 0$ and $D_xD_y < 0$. This is in contrast to a Sk existing only for $D_xD_y > 0$ region (or aSk existing only for $D_xD_y < 0$ region). This can be understood as follows.

Figure 10(a) shows a Bi sketch. To bridge bimerons shown in Fig. 6 and in the presented sketch, we mention that the "center" and "saddle" points in Fig. 6 corresponds to the segments with magnetization looking in positive and negative z-directions in Fig. 10. The Bi can be represented as two crossed 360-degree DWs. The first DW (along -45 degrees direction in Fig. 10(a)) has out-of-plane magnetization component and contributes to iDMI energy. Lets call it OOP DW. The second DW (directed by 45 degrees with respect to the x-axis in Fig. 10(a)) is in-plane. Lets call it IP DW. It has zero iDMI energy. This is due to the fact that the iDMI in thin films includes spatial derivatives of m_z (Eq. (1)), and magnetization rotation in the film plane gives zero average iDMI. Thus, only OOP DW defines the Bi stability. The Bi can orient in a way that the OOP DW has negative iDMI energy. At $D_x = D_y$ the Neel DW is favourable [56] leading to formation of "hedgehog" state in one of the Bi nodes (Fig. 10(a)). For $D_x = -D_y$ the iDMI favours the Bloch DW oriented by 45 degree to the x-axis [56]. Therefore, the Bi has a vortex node and is oriented by 45 degree. At that the iDMI contribution is negative and of the same order as for the case $D_x = D_y$. So, in both quadrants the iDMI can stabilized the Bi.

For Sk both DWs in orthogonal directions have out-of-plane magnetization component giving non-zero iDMI energy. In the case of $D_xD_y > 0$ both DW have negative iDMI leading to Sk stabilization. But for films with $D_xD_y < 0$, the DWs in perpendicular directions have iDMI energy of opposite sing "cancelling" each other. Therefore, the iDMI does not stabilize a Sk in $D_xD_y < 0$ region. Similarly, aSk cannot be stabilized by iDMI in $D_xD_y > 0$ region.

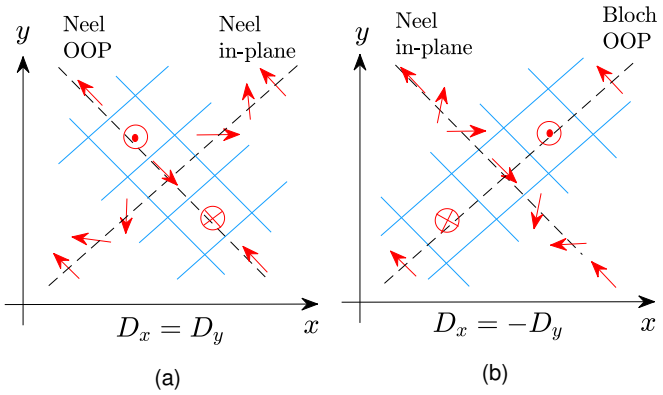

FIG. 10. Sketch of a Bi. (a) $D_x = D_y$. (b) $D_x = -D_y$.

The second peculiarity of the Bi stability diagram is that the stability region in $D_xD_y > 0$ quarter is different comparing to $D_xD_y < 0$ region. In particular, the upper bound for iDMI coefficients is lower in the $D_xD_y < 0$ quadrant. The Bi in the fourth quadrant ($D_xD_y < 0$) consists of the Bloch DWs. These DWs minimize the iDMI energy as well as the MD energy. At that in the $D_xD_y > 0$ region the DWs are of the Neel type minimizing only the iDMI energy but not the MD one. So, the energy of DWs of a Bi in $D_xD_y < 0$ quadrant is lower leading to earlier occurrence of instability as we increase the iDMI average strength.

IV. DISCUSSION

A. Control of topologically protected textures with strain

According to recent experiment [47] the iDMI anisotropy can be induced with anisotropic mechanical strain in the FM film. The strain can be created with an electric field in hybrid structures FM/ferroelectric (FE) as shown in Fig. 1. A voltage (applied to the FE) induces a deformation of the FE transferred to the FM film through the interface. The induced strain in the FM film in the hybrid structure can be as high as 0.3% [59]. This is a high enough value for essential variation of the iDMI [47]. Using FE $[Pb(Mg_{1/3}Nb_{2/3})O_3]_{0.66}[PbTiO_3]_{0.34}$ (PMN-PT) with a certain cut ([011]) one can induce the anisotropic strain in the FM film which induces the anisotropic iDMI. Thus, one can control the iDMI (and therefore topologically non-trivial magnetic textures) with an electric field.

B. Phenomenological description of the strain dependent iDMI

In our model we assume that iDMI has a particular symmetry, C_{2v}. In this section we show using symmetry arguments that this particular type of iDMI appears in the strained FM film.

We use an assumption about the system that the spatial inversion is broken at the FM/HM interface (which is the symmetry reason for iDMI existence). The magnitude of magnetization $\mathbf{m}(\mathbf{r})$ in the FM film has a fixed value and we consider $\mathbf{m}(\mathbf{r})$ as a unit vector. The FM film is thin and $\mathbf{m}(\mathbf{r})$ is uniform along the z-direction (perpendicular to the film plane).

In the most general form the iDMI is described using Lifshitz invariants

$$L_{ijk} = m_i \frac{\partial m_j}{\partial x_k} - m_j \frac{\partial m_i}{\partial x_k}. \tag{28}$$

For uniform magnetization along the z-axis the Lifshitz invariant L_{ijz} is absent. While there is no spatial inversion in the system other symmetries may exist. For zero strain we have reflection planes (xz) and (yz). In this case only two invariants are non-zero, L_{xzx} and L_{yzy}. For isotropic film the coefficients in front of these invariants are the same and we get

$$W^{(0)}_{\text{DMI}} = D_0(L_{xzz} + L_{yzy}) = \\ = D_0 \left(m_x \frac{\partial m_z}{\partial x} - m_z \frac{\partial m_x}{\partial x} + m_y \frac{\partial m_z}{\partial y} - m_z \frac{\partial m_y}{\partial y} \right), \tag{29}$$

where D_0 is the iDMI strength.

The strain applied to the film adds corrections to Eq. (29), $W^{(1)}_{\text{DMI}}$. The strain is described by the second order tensor u. We convolute it with the Lifshitz invariants and get

$$W^{(1)}_{\text{DMI}} = \alpha_{ijklm} u_{ij} L_{klm}. \tag{30}$$

Here α_{ijklm} is the 5-th order tensor describing the coupling between strain and iDMI. We consider the isotropic film with reflection planes perpendicular to the film plane. In this case many components of the tensor α_{ijklm} are zero. Using the film symmetry we obtain

$$W^{(1)}_{\text{DMI}} = \kappa_1 u_{zz}(L_{xzx} + L_{yzy}) + \\ + \kappa_2(u_{xx}L_{xzx} + u_{yy}L_{yzy}) + \kappa_3(u_{xx}L_{yzy} + u_{yy}L_{xzx}) + \\ + \kappa_4 u_{xy}(L_{xzy} + L_{yzx}) + \kappa_5(u_{xz}L_{xyy} - u_{yz}L_{xyx}). \tag{31}$$

It is hard to induce u_{zx} or u_{zy} strain components in thin films. The coordinate system can be always chosen in a way that $u_{xy} = 0$. Therefore, below we consider the case with only u_{xx} and u_{yy} components being finite. In this case the iDMI interaction is anisotropic and we find

$$W_{\text{DMI}} = W^{(0)}_{\text{DMI}} + W^{(1)}_{\text{DMI}} = D_x L_{xzz} + D_y L_{yzy} = \\ = D_x \left(m_x \frac{\partial m_z}{\partial x} - m_z \frac{\partial m_x}{\partial x} \right) + D_y \left(m_y \frac{\partial m_z}{\partial y} - m_z \frac{\partial m_y}{\partial y} \right), \tag{32}$$

where

$$D_x = D_0 + \kappa_1 u_{zz} + \kappa_2 u_{xx} + \kappa_3 u_{yy}, \\ D_y = D_0 + \kappa_1 u_{zz} + \kappa_2 u_{yy} + \kappa_3 u_{xx}. \tag{33}$$

V. CONCLUSION

We considered topologically non-trivial magnetic textures such as skyrmions, antiskyrmions and bimerons in thin magnetic films with anisotropic iDMI. Using micromagnetic simulations and analytical consideration we showed that iDMI anisotropy strongly affects stability, shape and internal structure of these textures. We obtain stability diagram of a single Sk and aSk in coordinates (D_x,D_y). A Sk can be stable when $D_xD_y > 0$, and aSk when $D_xD_y < 0$. The iDMI anisotropy reduces the range of iDMI strength in which these textures can exist. The iDMI anisotropy also makes Sk and aSk elliptic, however the ellipticity (ratio of main ellipse dimensions) is not big. Elliptic Sk and aSk are oriented along the main axes of the iDMI anisotropy. Due to the iDMI anisotropy the DW of a Sk and an aSk is reconfigured.

We also defined the stability diagram for a single Bi and aBi. Both these magnetic textures have the same stability conditions. In contrast to Sk and aSk, the iDMI anisotropy does not reduce the range of iDMI strength where Bi can exist. Therefore, a Bi exists in both regions $D_xD_y > 0$ and $D_xD_y < 0$. A Bi orientation and internal structure is also strongly affected by the iDMI anisotropy. In contrast to Sk and aSk, the Bi (aBi) orientation changes as we change the iDMI anisotropy. Depending on iDMI anisotropy the Bi can consist of vortex and antivortex or of "hedgehog" state and antivortex.

The iDMI anisotropy can be induced and tuned using strain. We developed a phenomenological theory of iDMI-strain coupling. In thin films the strain mostly induces the iDMI anisotropy. However, in specific conditions a new contribution to iDMI energy can be induced by strain. We consider these effects in a future.

VI. ACKNOWLEDGEMENTS

This research was supported by Center of Excellence "Center of Photonics" funded by The Ministry of Science and Higher Education of the Russian Federation, contract 075-15-2020-906. O. U. and I. B. were supported by NSF under Cooperative Agreement Award EEC-1160504.

[1] W. Jiang, G. Chen, K. Liu, J. Zang, S. G. te Velthuis, and A. Hoffmann, Physics Reports **704**, 1 (2017), skyrmions in Magnetic Multilayers.
[2] K. Everschor-Sitte, J. Masell, R. M. Reeve, and M. Klaui, Journal of Applied Physics **124**, 240901 (2018).
[3] B. Gobel, I. Mertig, and O. A. Tretiakov, Physics Reports (2020), https://doi.org/10.1016/j.physrep.2020.10.001.
[4] W. Sun, W. Wang, H. Li, G. Zhang, D. Chen, J. Wang, and Z. Cheng, Nature Communications **11**, 5930 (2020).
[5] R. Chen, C. Li, Y. Li, J. J. Miles, G. Indiveri, S. Furber, V. F. Pavlidis, and C. Moutafis, Phys. Rev. Applied **14**, 014096 (2020).
[6] X. Chen, W. Kang, D. Zhu, X. Zhang, N. Lei, Y. Zhang, Y. Zhou, and W. Zhao, Nanoscale **10**, 6139 (2018).
[7] X. Zhang, Y. Zhou, K. M. Song, T.-E. Park, J. Xia, M. Ezawa, X. Liu, W. Zhao, G. Zhao, and S. Woo, Journal of Physics: Condensed Matter **32**, 143001 (2020).
[8] S. Luo, N. Xu, Z. Guo, Y. Zhang, J. Hong, and L. You, IEEE Electron Device Letters **40**, 635 (2019).
[9] R. Saha, K. Wu, D. Su, and J.-P. Wang, Journal of Physics D: Applied Physics **52**, 465002 (2019).
[10] S. Li, W. Kang, X. Zhang, T. Nie, Y. Zhou, K. L. Wang, and W. Zhao, Mater. Horiz. , (2021).
[11] M. V. Sapozhnikov, S. N. Vdovichev, O. L. Ermolaeva, N. S. Gusev, A. A. Fraerman, S. A. Gusev, and Y. V. Petrov, Appl. Phys. Lett. **109**, 042406 (2016).
[12] M. V. Sapozhnikov, Journal of Magnetism and Magnetic Materials **396**, 338 (2015).
[13] C. Moreau-Luchaire, C. Moutafis, N. Reyren, J. Sampaio, C. A. F. Vaz, N. V. Horne, K. Bouzehouane, K. Garcia, C. Deranlot, P. Warnicke, P. Wohlhter, J.-M. George, M. Weigand, J. Raabe, V. Cros, and A. Fert, Nature Nanotechnology **11**, 444 (2016).
[14] G. Finocchio, F. Buttner, R. Tomasello, M. Carpentieri, and M. Klaui, Journal of Physics D: Applied Physics **49**, 423001 (2016).
[15] A. Fert, V. Cros, and Sampaio, Nature Nanotechnology **8**, 152 (2013).
[16] W. Jiang, P. Upadhyaya, W. Zhang, G. Yu, M. B. Jungfleisch, F. Y. Fradin, J. E. Pearson, Y. Tserkovnyak, K. L. Wang, O. Heinonen, S. G. E. te Velthuis, and A. Hoffmann, Science **349**, 283 (2015), https://science.sciencemag.org/content/349/6245/283.full.pdf.
[17] A. Fert, N. Reyren, and V. Cros, Nat. Rev. Mater. **2**, 17031 (2017).
[18] A. Soumyanarayanan, M. Raju, A. L. G. Oyarce, A. K. C. Tan, M.-Y. Im, A. P. Petrovi, P. Ho, K. H. Khoo, M. Tran, C. K. Gan, F. Ernult, and C. Panagopoulos, Nature Materials **16**, 904 (2017).
[19] A. N. Bogdanov, U. K. Rößler, M. Wolf, and K.-H. Müller, Phys. Rev. B **66**, 214410 (2002).
[20] M. Hoffmann, B. Zimmermann, G. P. Mller, D. Schrhoff, N. S. Kiselev, C. Melcher, and S. Blgel, Nature Communications **8**, 308 (2017).
[21] A. K. Nayak, V. Kumar, T. Ma, P. Werner, E. P. nad Roshnee Sahoo, F. Damay, U. K. Rler, C. Felser, and S. S. P. Parkin, Nature **548**, 561 (2017).
[22] W. Koshibae and N. Nagaosa, Nature Communications **5**, 5148 (2014).
[23] S. Huang, C. Zhou, G. Chen, H. Shen, A. K. Schmid, K. Liu, and Y. Wu, Phys. Rev. B **96**, 144412 (2017).
[24] L. Camosi, N. Rougemaille, O. Fruchart, J. Vogel, and S. Rohart, Phys. Rev. B **97**, 134404 (2018).
[25] X. Zhang, J. Xia, L. Shen, M. Ezawa, O. A. Tretiakov, G. Zhao, X. Liu, and Y. Zhou, Phys. Rev. B **101**, 144435 (2020).

[26] S.-Z. Lin, A. Saxena, and C. D. Batista, Phys. Rev. B **91**, 224407 (2015).
[27] Y. A. Kharkov, O. P. Sushkov, and M. Mostovoy, Phys. Rev. Lett. **119**, 207201 (2017).
[28] B. Göbel, A. Mook, J. Henk, I. Mertig, and O. A. Tretiakov, Phys. Rev. B **99**, 060407(R) (2019).
[29] S. K. Kim, Phys. Rev. B **99**, 224406 (2019).
[30] K.-W. Moon, J. Yoon, C. Kim, and C. Hwang, Phys. Rev. Applied **12**, 064054 (2019).
[31] R. Zarzuela, V. K. Bharadwaj, K.-W. Kim, J. Sinova, and K. Everschor-Sitte, Phys. Rev. B **101**, 054405 (2020).
[32] L. Shen, J. Xia, X. Zhang, M. Ezawa, O. A. Tretiakov, X. Liu, G. Zhao, and Y. Zhou, Phys. Rev. Lett. **124**, 037202 (2020).
[33] J. Ding, X. Yang, and T. Zhu, Journal of Physics D: Applied Physics **48**, 115004 (2015).
[34] Y.-H. Liu and Y.-Q. Li, Journal of Physics: Condensed Matter **25**, 076005 (2013).
[35] J. Müller and A. Rosch, Phys. Rev. B **91**, 054410 (2015).
[36] S.-Z. Lin, C. Reichhardt, C. D. Batista, and A. Saxena, Phys. Rev. B **87**, 214419 (2013).
[37] N. Romming, C. Hanneken, M. Menzel, J. E. Bickel, B. Wolter, K. von Bergmann, A. Kubetzka, and R. Wiesendanger, Science **341**, 636 (2013).
[38] G. Yu, P. Upadhyaya, X. Li, W. Li, S. K. Kim, Y. Fan, K. L. Wong, Y. Tserkovnyak, P. K. Amiri, and K. L. Wang, Nano Letters **16**, 1981 (2016).
[39] G. Yu, P. Upadhyaya, Q. Shao, H. Wu, G. Yin, X. Li, C. He, W. Jiang, X. Han, P. K. Amiri, and K. L. Wang, Nano Letters **17**, 261 (2017).
[40] W. Legrand, D. Maccariello, N. Reyren, K. Garcia, C. Moutafis, C. Moreau-Luchaire, S. Collin, K. Bouzehouane, V. Cros, and A. Fert, Nano Letters **17**, 2703 (2017).
[41] P.-J. Hsu, A. Kubetzka, A. Finco, N. Romming, K. von Bergmann, and R. Wiesendanger, Nature Nanotechnology **12**, 123 (2017).
[42] W. Kang, Y. Huang, C. Zheng, W. Lv, N. Lei, Y. Zhang, X. Zhang, Y. Zhou, and W. Zhao, Sci. Rep. **6**, 23164 (2016).
[43] X. Yao, J. Chen, and S. Dong, New Journal of Physics **22**, 083032 (2020).
[44] L. Qiu, J. Xia, Y. Feng, L. Shen, F. J. Morvan, X. Zhang, X. Liu, L. Xie, Y. Zhou, and G. Zhao, Journal of Magnetism and Magnetic Materials **496**, 165922 (2020).
[45] Y. Sun, Y. Ba, A. Chen, W. He, W. Wang, X. Zheng, L. Zou, Y. Zhang, Q. Yang, L. Yan, C. Feng, Q. Zhang, J. Cai, W. Wu, M. Liu, L. Gu, Z. Cheng, C.-W. Nan, Z. Qiu, Y. Wu, J. Li, and Y. Zhao, ACS Applied Materials & Interfaces **9**, 10855 (2017), pMID: 28266829, https://doi.org/10.1021/acsami.7b00284.
[46] Y. T. Yang, Q. M. Zhang, D. H. Wang, Y. Q. Song, L. Y. Wang, L. Y. Lv, Q. Q. Cao, and Y. W. Du, Applied Physics Letters **103**, 082404 (2013), https://doi.org/10.1063/1.4819459.
[47] N. S. Gusev, A. V. Sadovnikov, S. A. Nikitov, M. V. Sapozhnikov, and O. G. Udalov, Phys. Rev. Lett. **124**, 157202 (2020).
[48] O. G. Udalov and I. S. Beloborodov, Phys. Rev. B **102**, 134422 (2020).
[49] S. Rohart and A. Thiaville, Phys. Rev. B **88**, 184422 (2013).
[50] S. A. Osorio, M. B. Sturla, H. D. Rosales, and D. C. Cabra, Phys. Rev. B **99**, 064439 (2019).
[51] N. Nagaosa and Y. Tokura, Nat. Nanotechnol. **8**, 899 (2013).
[52] M. Donahue and D. Porter, *OOMMF User's Guide Version 1.0* (National Institute of Standards and Technology, Gaithersburg, MD, 1999).
[53] D. Cortes-Ortuno, M. Beg, V. Nehruji, L. Breth, R. Pepper, T. Kluyver, G. Downing, T. Hesjedal, P. H. adn T. Lancaster, R. Hertel, O. Hovorka, and H. Fangohr, New J. Phys. **20**, 113015 (2018).
[54] A. A. Fraerman, I. M. Nefedov, I. R. Karetnikova, M. V.Sapozhnikov, and I. A. Shereshevskii, Phys. Met. Metallogr. **92**, 226 (2001).
[55] E. D. Boerner and H. N. Bertran, IEEE Trans. Magn. **33**, 3052 (1997).
[56] O. Udalov and M. Sapozhnikov, Journal of Magnetism and Magnetic Materials **519**, 167464 (2021).
[57] J. A. Cape and G. W. Lehman, Journal of Applied Physics **42**, 5732 (1971).
[58] H. Callen and R. M. Josephs, Journal of Applied Physics **42**, 1977 (1971).
[59] H. Sohn, M. E. Nowakowski, C. yen Liang, J. L. Hockel, K. Wetzlar, S. Keller, B. M. McLellan, M. A. Marcus, A. Doran, A. Young, M. Klaui, G. P. Carman, J. Bokor, and R. N. Candler, ACS Nano **9**, 4814 (2015).